Hindawi
Journal of Spectroscopy
Volume 2021, Article ID 6684311, 8 pages
https://doi.org/10.1155/2021/6684311

Research Article

Pyrolysis and Morphology Behavior of EDTA-$Na_2Mg{\cdot}4H_2O$ and Coal Tar Pitch and Its Application for Porous Carbon

Wen-Juan Zhang,[1] **Shi-Hua Song**,[1] **and Wen-Hong Tian**[2]

[1]*School of Materials Science and Engineering, Jiujiang University, Jiujiang 332005, China*
[2]*Library of Jiujiang University, Jiujiang University, Jiujiang 332005, China*

Correspondence should be addressed to Wen-Juan Zhang; zhangwj_312@163.com

Received 22 October 2020; Revised 22 April 2021; Accepted 5 May 2021; Published 12 May 2021

Academic Editor: Carlos Palacio

Coal tar pitch (CTP) is a quite promising candidate for the production of porous carbons. Traditionally, the porous carbons are prepared by the heat treatment of carbon precursors in the presence of template and activator. In this paper, EDTA-$Na_2Mg{\bullet}4H_2O$ and CTP were mixed to produce porous carbons in the absence of template and activator, which were generated in situ by the heat treatment of EDTA-$Na_2Mg{\bullet}4H_2O$. The pyrolysis and morphology behavior of the mixture of EDTA-$Na_2Mg{\bullet}4H_2O$ and coal tar pitch (EDTA-$Na_2Mg{\bullet}4H_2O$@CTP) were studied by thermogravimetry and differential scanning calorimetry, Fourier transform infrared spectroscopy, X-ray diffraction, and scanning electron microscopy. The characteristics of the obtained porous carbons were characterized by N_2 adsorption-desorption isotherm. The results show that EDTA-$Na_2Mg{\bullet}4H_2O$ has a great influence on the pyrolysis and morphology of CTP. The pyrolysis behavior of CTP becomes complicated after the addition of EDTA-$Na_2Mg{\bullet}4H_2O$ for the physical and chemical changes of EDTA-$Na_2Mg{\bullet}4H_2O$ during the heat treatment. EDTA-$Na_2Mg{\bullet}4H_2O$@CTP dehydrates at 160°C and decomposes Na_2CO_3 and MgO at 600°C. The surface morphology of EDTA-$Na_2Mg{\bullet}4H_2O$@CTP changes with the EDTA-$Na_2Mg{\bullet}4H_2O$ content and heat treatment temperature. After acid washing of the product of EDTA-$Na_2Mg{\bullet}4H_2O$@CTP heat-treated at 700°C, the obtained porous carbon material consists of micropores and mesopores. Its specific surface area is 574.18 $m^2\,g^{-1}$ and the average pore width is 4.53 nm.

1. Introduction

Carbon materials are promising candidates for supercapacitor because of their chemical stability, low cost, fine conductivity, and versatile existing forms [1]. Porous carbon, one of the most important carbon materials, is of great importance for its high specific capacitance [2–5]. Various methods were adopted to synthesize porous carbons, such as chemical activation, physical activation, the combination of physical and chemical activation processes [6–8], and newly developed template-synthesized mesoporous/microporous carbons [9–15].

Various carbon materials were prepared from different raw materials and by different methods. Hierarchical porous carbon with a large surface area of 3188 $m^2\,g^{-1}$ and a pore volume of 3.2 $cm^3\,g^{-1}$ was prepared by the sol-gel process of lotus seed shell and sodium phytate, followed by carbonization and NaOH activation [16]. Alginate-derived porous carbon was obtained by the nano-ZnO hard template-induced $ZnCl_2$ activation method [17]. It has a well-developed hierarchical porous structure and its specific surface area is up to 2589 $m^2\,g^{-1}$. Nitrogen-doped hierarchical porous carbon was prepared from polyaniline/silica self-aggregates, and its specific surface area is 899 $m^2\,g^{-1}$ [18]. A hierarchically porous carbon was prepared via a facile hard-templating method using silica as a template, which is thoroughly removed by an in situ polytetrafluoroethylene pyrolytic process without further treatment. The specific surface area can reach up to 664 $m^2\,g^{-1}$ [19]. Cattail wool-derived porous carbon was fabricated by using calcium carbonate as a hard template and potassium oxalate monohydrate as activation [20]. High-quality meso/micropore-

controlled hierarchical porous carbon was synthesized by a hard template method utilizing rice husk biochar and then used to adsorb copper ions from an aqueous solution [21].

Coal tar pitch (CTP) is a kind of complex material consisting of aromatic compounds with a broad molecular weight distribution [22]. It is a quite promising candidate for the production of porous carbons for its low cost, abundant resources, and the ability to generate graphitizable carbons [23]. In this paper, CTP was used as a carbon material precursor to produce porous carbons in the presence of EDTA-$Na_2Mg\bullet 4H_2O$, which decomposes CO_2, Na_2CO_3. and MgO at high temperatures and the products can be used as activators and templates for porous carbon materials. The pyrolysis and morphology behavior of the mixture of EDTA-$Na_2Mg\bullet 4H_2O$ and coal tar pitch (EDTA-$Na_2Mg\bullet 4H_2O$@ CTP) was studied, and the obtained porous carbon was characterized.

2. Experiment

2.1. Materials. CTP, the softening point of which is 108°C, was purchased from the Wuhan Iron and Steel Co. Ltd. (Wuhan, China) and its toluene insoluble and quinoline insoluble content were 43% and 6.8%, respectively. The EDTA-$Na_2Mg\bullet 4H_2O$ used in the experiment was of analytical grade and provided by Nanjing Duly Biotech Co. Ltd. (Nanjing, China).

2.2. Preparation of Materials. For a typical run, CTP with a particle size of below 100 um and EDTA-$Na_2Mg\bullet 4H_2O$ were used as raw materials. Their mixture process was carried out in a traditional ball mill at a rotation rate of 450 rpm for 2 h. The obtained mixture is named as MM-*a*-*b*, where *a* is the mass of EDTA-$Na_2Mg\bullet 4H_2O$ and *b* is the mass of CTP.

2.3. Heat Treatment and Acid Cleaning Treatment. Heat treatment of the MM-8-1 was carried out in a tube furnace. About 5 g sample was heated to a designated temperature at a rate of 4 °C min^{-1} and kept at this temperature for 1 hour. The N_2 stream was introduced into the tube furnace throughout the carbonization. In this paper, the samples were heated to 500°C, 600°C, 700°C, and 800°C and cooled to room temperature. The resulting products are denoted as MM-8-1-*t*, where *t* stands for the heat treatment temperature.

The MM-8-1-800 was then washed with HCl solution (6 mol L^{-1}) and stirred for 4 h. Finally, it was filtered and washed thoroughly with distilled water and ethanol to remove the residual ions and byproducts and then dried in an oven at 110°C. The as-obtained porous carbon is nominated as PC-8-1-800.

2.4. Measurements. Thermogravimetry and differential scanning calorimetry analysis (TG-DSC) was performed on a thermal analyzer (model Pyris Diamond, Perkin-Elmer, USA) under an N_2 atmosphere with a heating rate of 10°C min^{-1}. Fourier transform infrared (FT-IR) spectroscopy was acquired on a Thermo Nicolet-360 FT-IR spectrometer in the range of 4000–400 cm^{-1}. X-ray diffraction (XRD) was carried out on the PANalytical X'Pert PRO X-ray diffraction instrument with CuKα ($\lambda = 1.5406$ Å) radiation at 40 kV and 35 mA. The morphologies of the samples were examined using TESCAN VEGA II scanning electron microscopy (SEM). The N_2 adsorption/desorption isotherms at −196°C were measured using a Micromeritics TriStar 3020 porosimeter. Specific surface area (SSA) was calculated by the Brunauer–Emmett–Teller (BET) method and pore size distributions were analyzed by the Barrett–Joyner–Halenda (BJH) method.

3. Results and Discussion

3.1. TG-DSC Analysis. Figure 1 shows the TG-DSC curves of parent CTP and MM-8-1. It can be seen from the TG-DSC curve of parent CTP that it decomposes in one single mass loss stage in the temperature range of 25–900°C. The weight loss is mainly due to the removal of gases and light compounds generated via thermal polymerization and the cracking of side chains of aromatic rings [22]. The DSC profile of parent CTP is characterized by a small endothermic peak at about 60°C, two exothermic peaks close together at about 530°C, and a big exothermic peak at 640°C. The peak at about 60°C, which is not accompanied by weight loss, indicates the state of CTP transformed from brittle to viscoelasticity [24]. The three exothermic peaks at about 530°C and 640°C, which are associated with weight loss during the heat treatment process, are corresponding to the reactions of thermal polymerization taken place at these temperatures [24].

For MM-8-1, the TG-DSC curve becomes complicated. The slope of the TG curve becomes steep in the temperature range of 140–200°C and the corresponding DSC curve at this stage has an endothermic peak, which corresponds to the removal of crystal water from EDTA-$Na_2Mg\bullet 4H_2O$. Further, the TG-DSC curve becomes complicated in the temperature range of 200–450°C. There is a large exothermic peak at 408°C, and the thermal weight loss rate at this temperature is the largest, indicating that violent and complex physical and chemical reactions occur at this stage. At last, in the temperature range of 450–900°C, the DSC curve shows two endothermic peaks at 500°C and 858°C and two exothermic peaks at 564°C and 805°C, indicating that physical or chemical reaction occurs in the system at these temperatures.

3.2. FT-IR Analysis. To explore the structural changes of MM-8-1 during the pyrolysis, the raw materials and the products of MM-8-1 heat-treated at 500°C, 600°C, 700°C, and 800°C are characterized by FT-IR, which are illustrated in Figure 2. The attribution of the peaks in FT-IR spectra is listed in Table 1. From Figure 2, it can be observed the FT-IR spectrum of MM-8-1 is the superposition of CTP and EDTA-$Na_2Mg\bullet 4H_2O$. During the pyrolysis of MM-8-1, the peak at about 3345 cm^{-1}, which is attributed to O–H stretching vibration, disappears when it is heated to a temperature higher than 500°C. Otherwise, the peak at

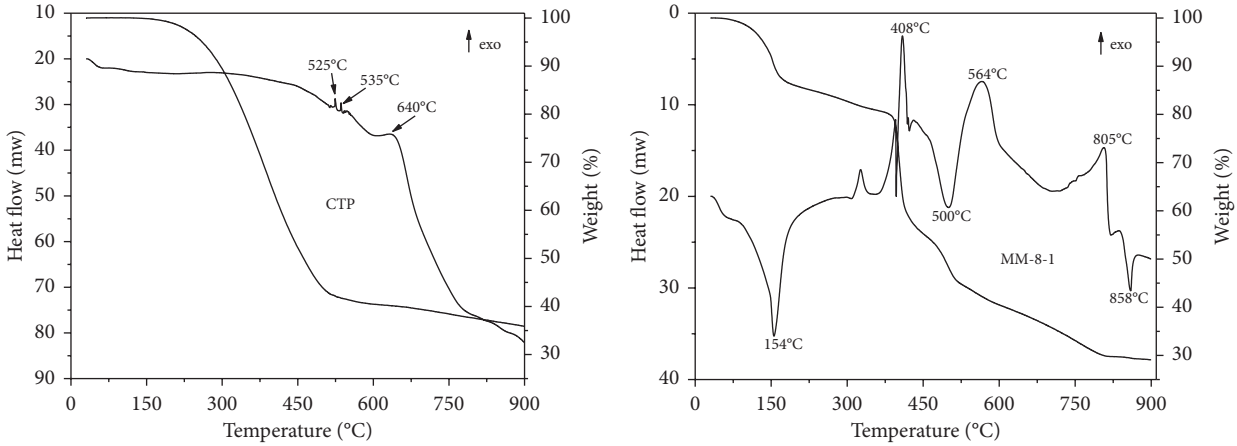

Figure 1: TG-DSC curves of parent CTP and MM-8-1.

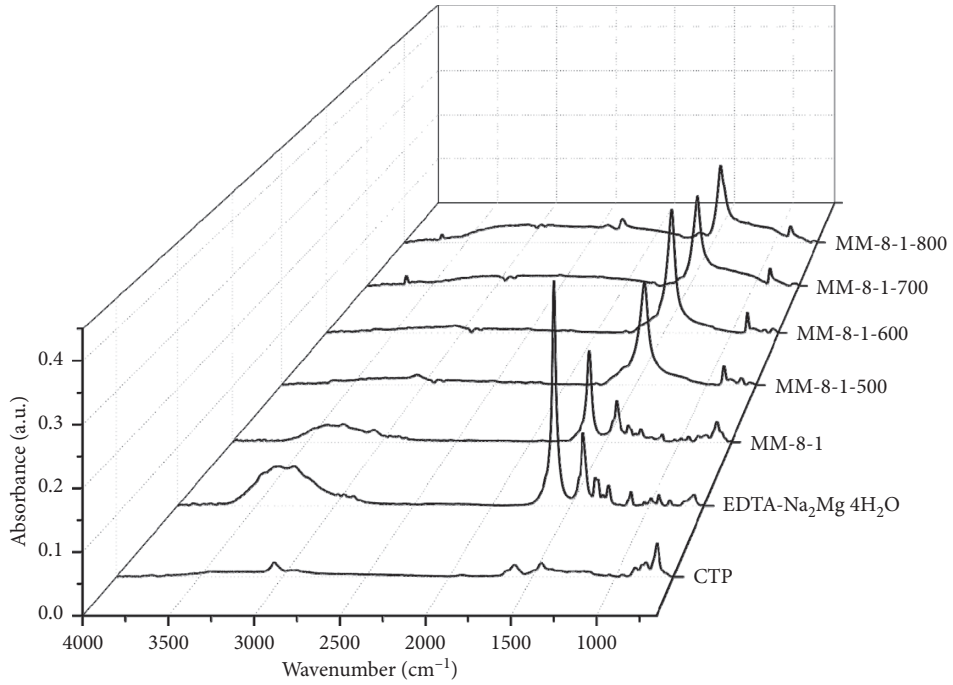

Figure 2: FT-IR spectra of raw materials and the cokes of MM-8-1 heat-treated at different temperatures.

Table 1: The attribution of the peaks in the FT-IR spectra.

Wavenumber (cm^{-1})	Attribution
3420	O–H stretching vibration.
3030	Aromatic C–H stretching vibration
1600	C=C stretching vibration [25]
1441	C–H bending vibration of methyl and methylene
700–900	Aromatic out-of-plane C–H vibration with different substitution patterns
750	Out-of-plane bending vibration with four adjacent hydrogens on aromatic rings [26]

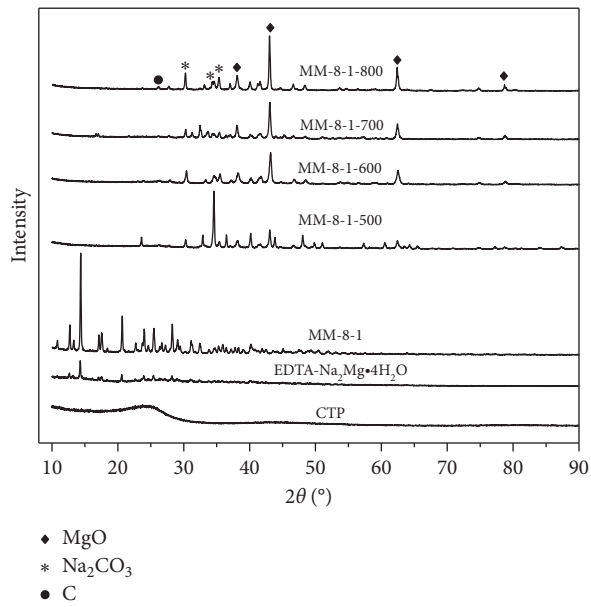

Figure 3: XRD patterns of raw materials and the cokes of MM-8-1 heat-treated at different temperatures.

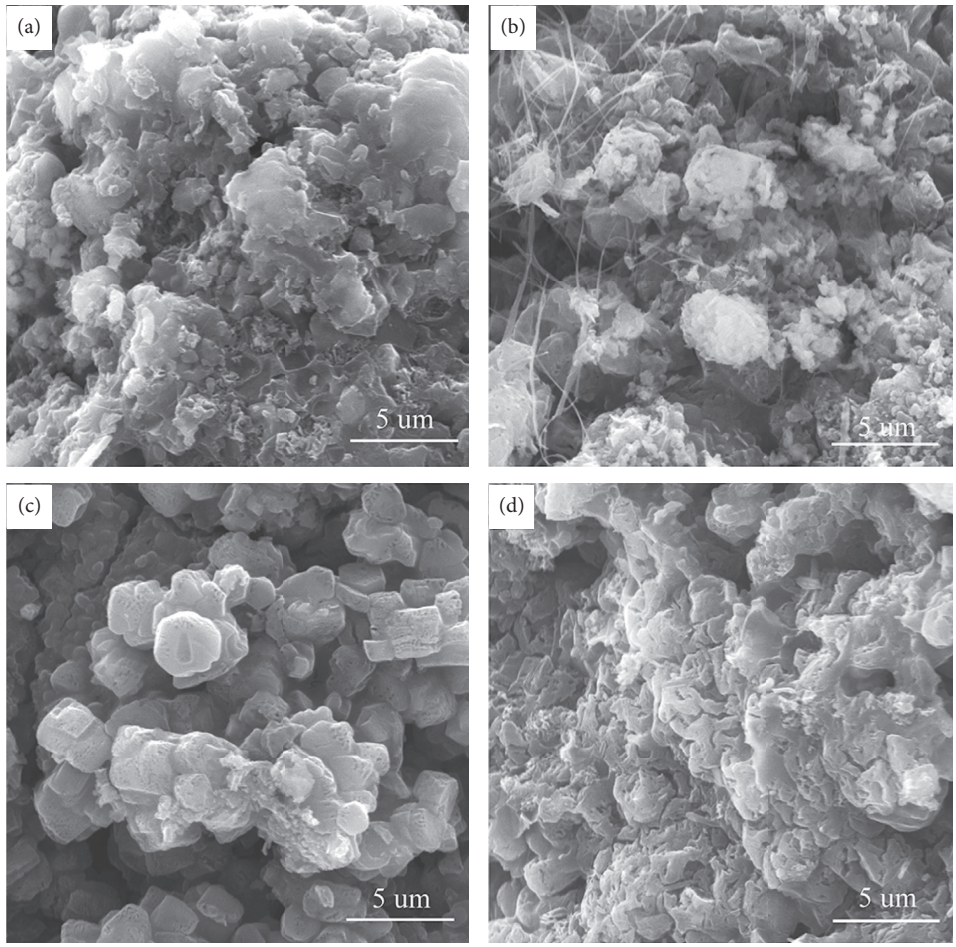

Figure 4: Effect of EDTA-$Na_2Mg\bullet 4H_2O$ content on the morphology of CTP (a) MM-4-1-600; (b) MM-6-1-600; (c) MM-8-1-600; (d) MM-10-1-600.

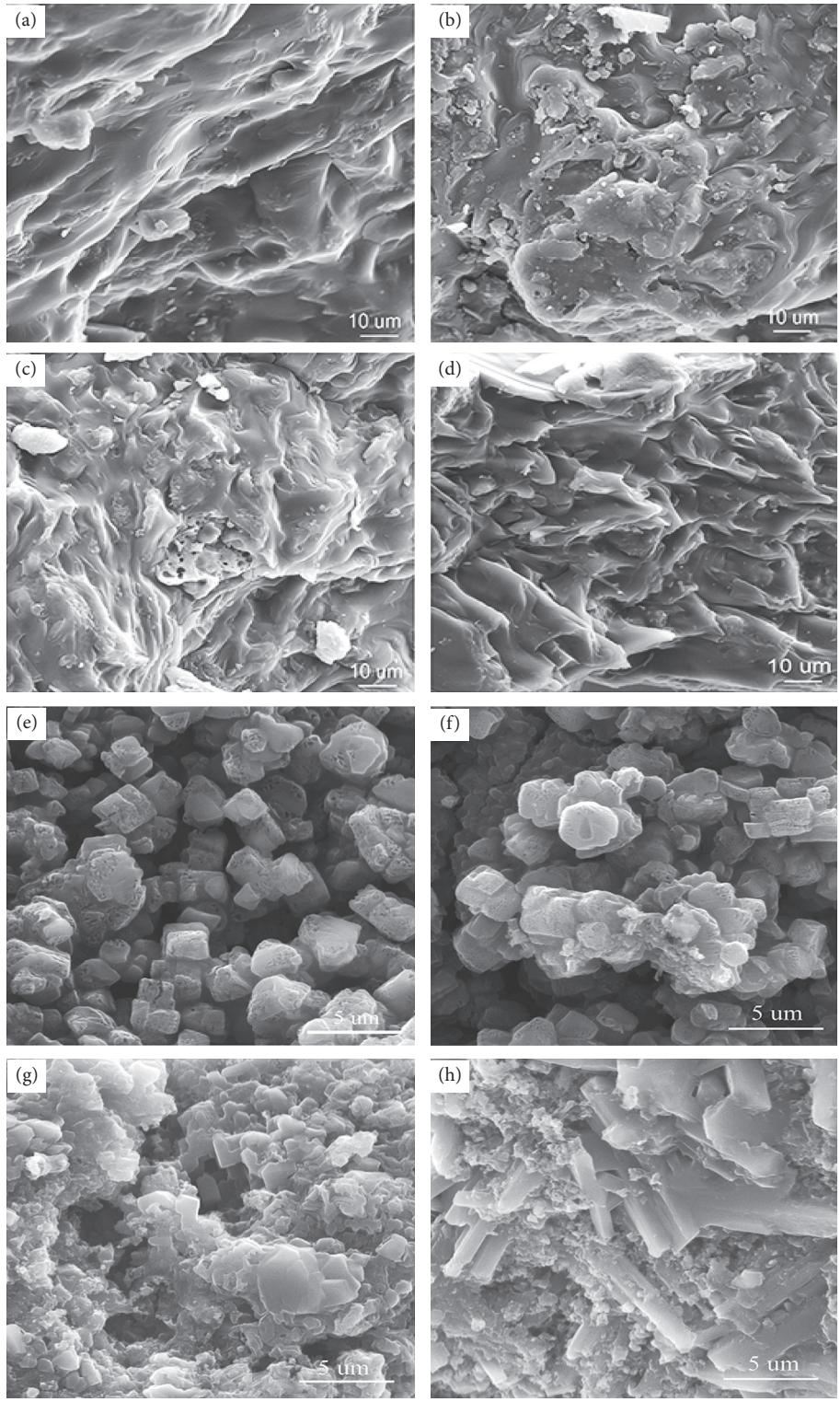

Figure 5: Effect of the heat treatment temperature on the morphology of parent CTP and MM-8-1. (a) Parent CTP-500; (b) parent CTP-600; (c) parent CTP-700; (d) parent CTP-800; (e) MM-8-1-500; (f) MM-8-1-600; (g) MM-8-1-700; (h) MM-8-1-800.

750 cm^{-1}, which corresponds to the out-of-plane bending vibration with four adjacent hydrogens on aromatic rings, becomes small with the increase of heat treatment temperature. The peak at about 1600 cm^{-1} disappears after it is heated to a temperature higher than 500°C, and the intensity of the peak at 1420 cm^{-1} enhances with the increasing

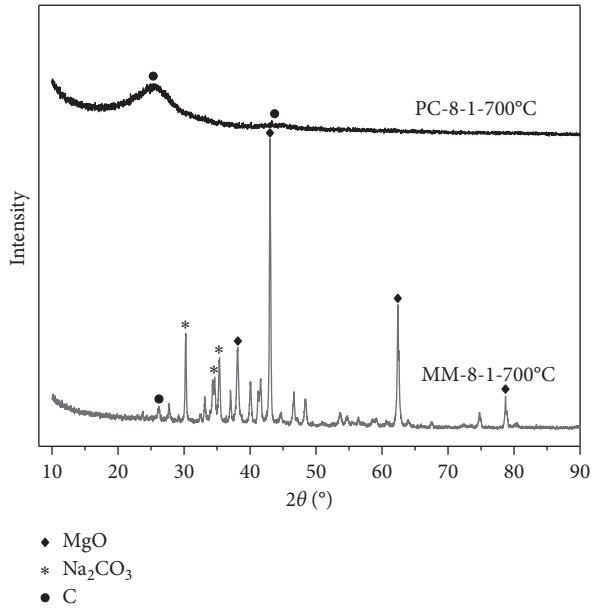

Figure 6: XRD patterns of MM-8-1-700 and PC-8-1-700.

temperature. Further, there is little difference for the FT-IR spectra of MM-8-1-500, MM-8-1-600, MM-8-1-700, and MM-8-1-800.

3.3. XRD Analysis. In order to further determine the physical and chemical changes during the heat treatment of MM-8-1, all the samples were characterized by XRD, as shown in Figure 3. It can be seen that there are many peaks in the raw material of MM-8-1, including XRD diffraction peaks of EDTA-Na_2Mg•$4H_2O$ and carbon. With the increase of temperature, the decomposition reaction of EDTA-Na_2Mg•$4H_2O$ occurs. When the temperature is higher than 600°C, all the samples only show the peaks of Na_2CO_3, MgO, and C. In addition, with the increase of temperature, the intensity of diffraction peak further increased, indicating that the crystallinity of corresponding products increased. Combined with the results of TG-DSC, it can be concluded that EDTA-Na_2Mg•$4H_2O$ has the following reactions with the increase of temperature.

$$\mathrm{EDTANa_2Mg \cdot 4H_2O} \xrightarrow[160°\mathrm{C}]{\Delta} \mathrm{EDTANa_2Mg + 4H_2O} \quad (1)$$

$$\mathrm{EDTANa_2Mg} \xrightarrow[600°\mathrm{C}]{\Delta} \mathrm{Na_2CO_3 + MgO + CO_2} \quad (2)$$

3.4. SEM Analysis. In order to study the influence of EDTA-Na_2Mg•$4H_2O$ content on the surface morphology of CTP, MM-4-1, MM-6-1, MM-8-1, and MM-10-1 were heated to 600°C and kept for 1 hour. The SEM image of the products is shown in Figure 4. It can be seen from the figure that when the ratio of EDTA-Na_2Mg•$4H_2O$ to CTP is 4 : 1, the surface morphology is like a layered petal (see Figure 4(a)). As the ratio increases, filaments are formed in the system (see Figure 4(b)). When the ratio of EDTA-Na_2Mg•$4H_2O$ to CTP is 8 : 1, the surface morphology is a relatively regular block, and the size of the block is about 2.5 um (see Figure 4(c)). When the concentration continues to increase, the blocks disappear, forming a relatively dense uneven surface (see Figure 4(d)). It can be concluded that, with the increase of EDTA-Na_2Mg•$4H_2O$ content, the Na_2CO_3 and CO_2 in the pyrolysis process of the system continue to increase, and the activation effect on the system is continuously enhanced and leads to the change of the morphology.

Figure 5 shows the surface morphology of parent CTP and MM-8-1 heat-treated at 500°C, 600°C, 700°C, and 800°C. It can be observed the surfaces of parent CTP change greatly with the increase of temperature. When it is heated to 500°C, the surface becomes relatively neat (see Figure 5(a)). However, the surface becomes messy when it is heated to 600°C and 700°C (see Figures 5(c) and 5(d)), which may be caused by the reaction of thermal polymerization taken place at about 530°C. In addition, some pores exist on the surface of parent-700 (see Figure 5(c)). When it is heated to 800°C, the surface is arranged in a relatively orderly manner.

For MM-8-1, the surface morphology is different from that of parent CTP at the same heat treatment temperature. When it is heated to 500°C and 600°C, some rock sugar lumps with a particle size of about 1–3 μm are generated (see Figures 5(e) and 5(f)). When the temperature is higher than 600°C, the resulting material appears fluffy (see Figures 5(g) and 5(h)). It can be inferred that as the temperature increases, the reaction speed increases, leading to the activated substances in the system increase, and the morphology changes.

3.5. Characteristics of PC-8-1-700. Figure 6 shows the XRD patterns of MM-8-1-700 before and after acid washing. It can be seen that only the diffraction peak of C exists after washing, indicating that Na_2CO_3 and MgO have been

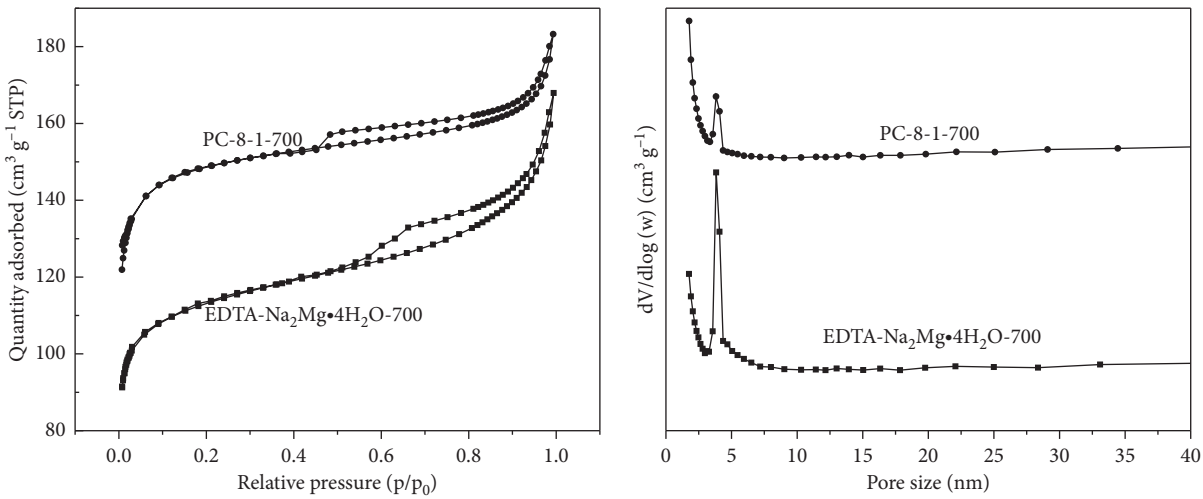

Figure 7: The N_2 adsorption-desorption isotherm and the BJH pore size distribution of PC-8-1-700 and EDTA-Na_2Mg•$4H_2O$-700.

Table 2: Pore structure parameters of PC-8-1-700 and EDTA-Na_2Mg•$4H_2O$-700.

	S_{BET} (m^2 g^{-1})[a]	V_t (cm^3 g^{-1})[b]	V_{mic} (cm^3 g^{-1})[c]	D_{ap} (nm)[d]
EDTA-Na_2Mg•$4H_2O$-700	436.95	0.25	0.13	5.22
PC-8-1-700	574.18	0.28	0.19	4.53

[a]BET surface area. [b]The total pore volume by single point method. [c]t-plot micropore volume. [d]BJH desorption average pore width.

thoroughly cleaned. The chemical reaction equations involved are shown as follows:

$$Na_2CO_3+2HCl = 2NaCl + H_2O + CO_2\uparrow \quad (3)$$

$$MgO + 2HCl = MgCl_2+H_2O \quad (4)$$

The N_2 adsorption and desorption isotherms of PC-8-1-700 and EDTA-Na_2Mg•$4H_2O$-700 are shown in Figure 7. It can be seen that they are typical type IV isotherm and have strong N_2 adsorption under low pressure ($P/P_0 \leq 0.35$), indicating that the materials have a strong force with nitrogen. With the increase of relative pressure, the adsorption and desorption capacity of nitrogen are obviously different. The adsorption and desorption curves cannot coincide and hysteresis loops appear, which indicates that there are a lot of micropores and mesopores in the materials. Meanwhile, the pore size distribution in Figure 7(b) also proves the coexistence of micropores and mesopores in the materials. The pore structure parameters of all the samples are summarized in Table 2. The specific surface area (S_{BET}) of EDTA-Na_2Mg•$4H_2O$-700 and PC-8-1-700 is 436.95 and 574.18 m^2 g^{-1}, while the total pore volume (V_t) is 0.25 and 0.28 cm^3 g^{-1}, and the micropore volume (V_{mic}) is 0.13 and 0.19 cm^3 g^{-1}, respectively. The increase of the surface area and pore volume may be caused by the complicated physical changes between EDTA-Na_2Mg•$4H_2O$ and coal pitch at high temperature and the decomposition of EDTA-Na_2Mg•$4H_2O$ at high temperature to form magnesium oxide, which is washed away by hydrochloric acid.

4. Conclusions

EDTA-Na_2Mg•$4H_2O$@CTP decomposes MgO, Na_2CO_3, and CO_2 at 600°C and the thermal reduction of MgO and C occurs at about 858°C. For the physical and chemical changes of EDTA-Na_2Mg•$4H_2O$, it has a great influence on the pyrolysis and morphology of CTP. After acid washing of the carbon material heat-treated at 700°C, the obtained porous carbon material consists of micropores and mesopores. Its specific surface area is 574.18 m^2 g^{-1} and the average pore diameter is 4.53 nm.

Data Availability

The data used to support the findings of this study are available from the corresponding author upon request.

Conflicts of Interest

The authors declare that there are no conflicts of interest regarding the publication of this paper.

Acknowledgments

This research was supported by the Science and Technology Project of Department of Education of Jiangxi Province (GJJ170948).

References

[1] H. Guo and Q. Gao, "Boron and nitrogen co-doped porous carbon and its enhanced properties as supercapacitor," *Journal of Power Sources*, vol. 186, no. 2, pp. 551–556, 2009.

[2] S. Lin, L. Mo, and F. Wang, "One-step synthesis of O-self-doped honeycomb-like hierachically porous carbons for supercapacitors," *Journal of Electrochemical Energy Conversion and Storage*, vol. 19, no. 1, Article ID 011004, 2021.

[3] Y. He, Z. Cheng, H. Zuo, C. Yan, and Y. Liao, "Green synthesis of pyridyl conjugated microporous polymers as precursors for porous carbon microspheres for efficient electrochemical energy storage," *Chemelectrochem,*vol. 7, no. 4, 2020.

[4] D. Zhang, Y. Xue, J. Chen et al., "N, S, O self-doped porous carbon nanoarchitectonics derived from pinecone with outstanding supercapacitance performances," *Journal of Nanoscience and Nanotechnology*, vol. 20, no. 5, pp. 2728–2735, 2020.

[5] A. Lzs, A. Yyz, B. Bqh, A. Zpx, B. Llj, and C. Zjf, "N-doped layered porous carbon electrodes with high mass loadings for high-performance supercapacitors," *New Carbon Materials,*vol. 36, no. 1, pp. 179–188, 2021.

[6] X. Gang, M. Krishnamoorthy, W. Jiang, J. Pan, Z. Pan, and X. Liu, "A novel in-situ preparation of N-rich spherical porous carbon as greatly enhanced material for high-performance supercapacitors," *Carbon*, vol. 171, pp. 62–71, 2021.

[7] Q. Wang, J. Yan, T. Wei et al., "Two-dimensional mesoporous carbon sheet-like framework material for high-rate supercapacitors," *Carbon*, vol. 60, pp. 481–487, 2013.

[8] B. Petrova, B. Tsyntsarski, T. Budinova et al., "Synthesis of nanoporous carbons from mixtures of coal tar pitch and furfural and their application as electrode materials," *Fuel Processing Technology*, vol. 91, no. 11, pp. 1710–1716, 2010.

[9] X. He, H. Zhang, H. Zhang, X. Li, N. Xiao, and J. Qiu, "Direct synthesis of 3D hollow porous graphene balls from coal tar pitch for high performance supercapacitors," *Journal of Materials Chemistry A*, vol. 2, no. 46, pp. 19633–19640, 2014.

[10] X. Zhang, S. Luo, Q. Lin, Y. Wang, X. Huang, and L. Xiong, "Effect of carbothermal reduction on the microstructures of porous carbons from the mixture of coal-tar pitch and nano-MgO," *Journal of Analytical and Applied Pyrolysis*, vol. 124, pp. 73–78, 2017.

[11] J. Zhang, L. Jin, J. Cheng, and H. Hu, "Hierarchical porous carbons prepared from direct coal liquefaction residue and coal for supercapacitor electrodes," *Carbon*, vol. 55, pp. 221–232, 2013.

[12] L. Wang, J. Wang, F. Jia, C. Wang, and M. Chen, "Nanoporous carbon synthesised with coal tar pitch and its capacitive performance," *Journal of Materials Chemistry A*, vol. 1, no. 33, pp. 9498–9507, 2013.

[13] W. Teng, Y. Zhong, and R. Liu, "Synthesis of ordered mesoporous carbons by Teflon-assisted removal of silica template in tri-constituent co-assembly for supercapacitors," *Emergent Materials*, vol. 3, no. 3, pp. 339–346, 2020.

[14] X. Wang, S. Chen, J. Sun, D. Zhang, and J. Song, "Synthesis of large pore sized mesoporous carbon using alumina-templated strategy for high-performance RhB removal," *Microporous and Mesoporous Materials*, vol. 318, Article ID 110993, 2021.

[15] Y. Liu, P. Li, Y. Wang et al., "A green and template recyclable approach to prepare Fe3O4/porous carbon from petroleum asphalt for lithium-ion batteries," *Journal of Alloys and Compounds*, vol. 695, pp. 2612–2618, 2017.

[16] L. Hu, Q. Zhu, Q. Wu, D. Li, Z. An, and B. Xu, "Natural biomass-derived hierarchical porous carbon synthesized by an in situ hard template coupled with NaOH activation for ultrahigh rate supercapacitors," *ACS Sustainable Chemistry & Engineering*, vol. 6, no. 11, pp. 13949–13959, 2018.

[17] L. Qin, Z. Xiao, S. Zhai, S. Wang, and Q. An, "Alginate-derived porous carbon obtained by nano-ZnO hard template-induced $ZnCl_2$-activation method for enhanced electrochemical performance," *Journal of the Electrochemical Society,*vol. 167, 2020.

[18] P. Li, D. Zhang, Y. Xu, C. Ni, G. Shi, and X. Sang, "Nitrogen-doped hierarchical porous carbon from polyaniline/silica self-aggregates for supercapacitor," *Chinese Journal of Chemical Engineering*, vol. 27, no. 3, pp. 709–716, 2019.

[19] X. Wu, H. Li, X. Yang, X. Wang, and S. Zhuo, "Polytetrafluoroethylene-assisted removal of hard-template to prepare hierarchically porous carbon for high energy density supercapacitor with KI-additive electrolyte," *Electrochimica Acta,*vol. 368, Article ID 137610, 2021.

[20] Y. A. Jie, A. Qt, Z. A. Ye, and A. X. Xyw, "Facile synthesis and superior capacitive behavior of cattail wool-derived hierarchical porous carbon," *Journal of Electroanalytical Chemistry*, vol. 882, Article ID 115025, 2021.

[21] V. Dinh, "Meso/micropore-controlled hierarchical porous carbon derived from activated biochar as a high-performance adsorbent for copper removal," *Science of the Total Environment,*vol. 692, pp. 844–853, 2019.

[22] M. Pérez, M. Granda, R. Santamaría, T. Morgan, and R. Menéndez, "A thermoanalytical study of the co-pyrolysis of coal-tar pitch and petroleum pitch," *Fuel*, vol. 83, no. 9, pp. 1257–1265, 2004.

[23] Y.-X. Wang, S.-L. Chou, J. H. Kim, H.-K. Liu, and S.-X. Dou, "Nanocomposites of silicon and carbon derived from coal tar pitch: cheap anode materials for lithium-ion batteries with long cycle life and enhanced capacity," *Electrochimica Acta*, vol. 93, pp. 213–221, 2013.

[24] D. Mikociak, A. Magiera, G. Labojko, and S. Blazewicz, "Effect of nanosilicon carbide on the carbonisation process of coal tar pitch," *Journal of Analytical and Applied Pyrolysis*, vol. 107, no. 9, pp. 191–196, 2014.

[25] R. M. Balabin, R. Z. Syunyaev, T. Schmid, J. Stadler, E. I. Lomakina, and R. Zenobi, "Asphaltene adsorption onto an iron surface: combined near-infrared (NIR), Raman, and AFM study of the kinetics, thermodynamics, and layer structure," *Energy & Fuels*, vol. 25, no. 1, pp. 189–196, 2011.

[26] J. Alcañiz-Monge, D. Cazorla-Amorós, and A. Linares-Solano, "Characterisation of coal tar pitches by thermal analysis, infrared spectroscopy and solvent fractionation," *Fuel*, vol. 80, no. 1, pp. 41–48, 2001.